

# Comparison of Cirrus Cloud Radiative Properties and Dynamical Processes at Two Atmospheric Radiation Measurement Sites in the Tropical Western Pacific

*J. M. Comstock, J. H. Mather, and T. P. Ackerman  
Pacific Northwest National Laboratory  
Richland, Washington*

## Introduction

Upper tropospheric humidity plays an important role in the formation and maintenance of tropical cirrus clouds. Deep convection is crucial for the transport of water vapor from the boundary layer to the upper troposphere and is responsible for the formation of anvil cirrus that can spread horizontally over considerable distances and persist for several hours. In addition, recent studies have linked large-scale stratospheric dynamics to the presence of tropical cirrus clouds that are not necessarily linked directly with deep convection. In this study, we use ground-based remote sensing measurements, obtained from the U. S. Department of Energy, Atmospheric Radiation Measurement (ARM) sites located on Manus and Nauru Islands, to retrieve cirrus properties, such as cloud height, thickness, and visible optical depth. We then examine differences in top of the atmosphere (TOA) and surface radiation budgets observed at each site, which helps determine the amount of convective activity that influences each location. Comparisons of cloud properties also reveal the influence of deep convection and large-scale dynamics on cirrus radiative properties.

## Overview of the Tropical Western Pacific

Manus (1.058°S, 147.425°E) and Nauru (0.521°S, 166.916°E) islands are located in the Tropical Western Pacific (TWP). When studying the differences in cloud properties between Manus and Nauru, it is useful to consider the large-scale environment in which these islands are embedded. Figures 1 and 2 provide two different views of the TWP region that put Manus and Nauru in a larger context. Monthly mean outgoing longwave radiation (OLR) from National Centers for Environmental Prediction (NCEP) data (Figure 1) show that, with rare exceptions (such as the 1997 El Nino), Manus is in a convectively active region (indicated by low OLR values) while Nauru is much more variable. Since the 1997 El Nino, Nauru has experienced convectively suppressed conditions; however, measurements indicate that OLR is decreasing as low OLR values shift toward the East during 2001-2002 (Figure 1).

A snapshot of the 1000-hPa horizontal divergence from European Centre for Medium-Range Weather Forecasts (ECMWF) analysis (Figure 2) taken from November 1999 show the large-scale patterns of convection in the Western Pacific. Two semi-permanent regions of convection dominate the region, the inter-tropical convergence zone (ITCZ) that runs East to West between 5° and 10°N, and the South Pacific convergence zone (SPCZ) that runs from Papua New Guinea (5°S to 140°E) to the southeast,

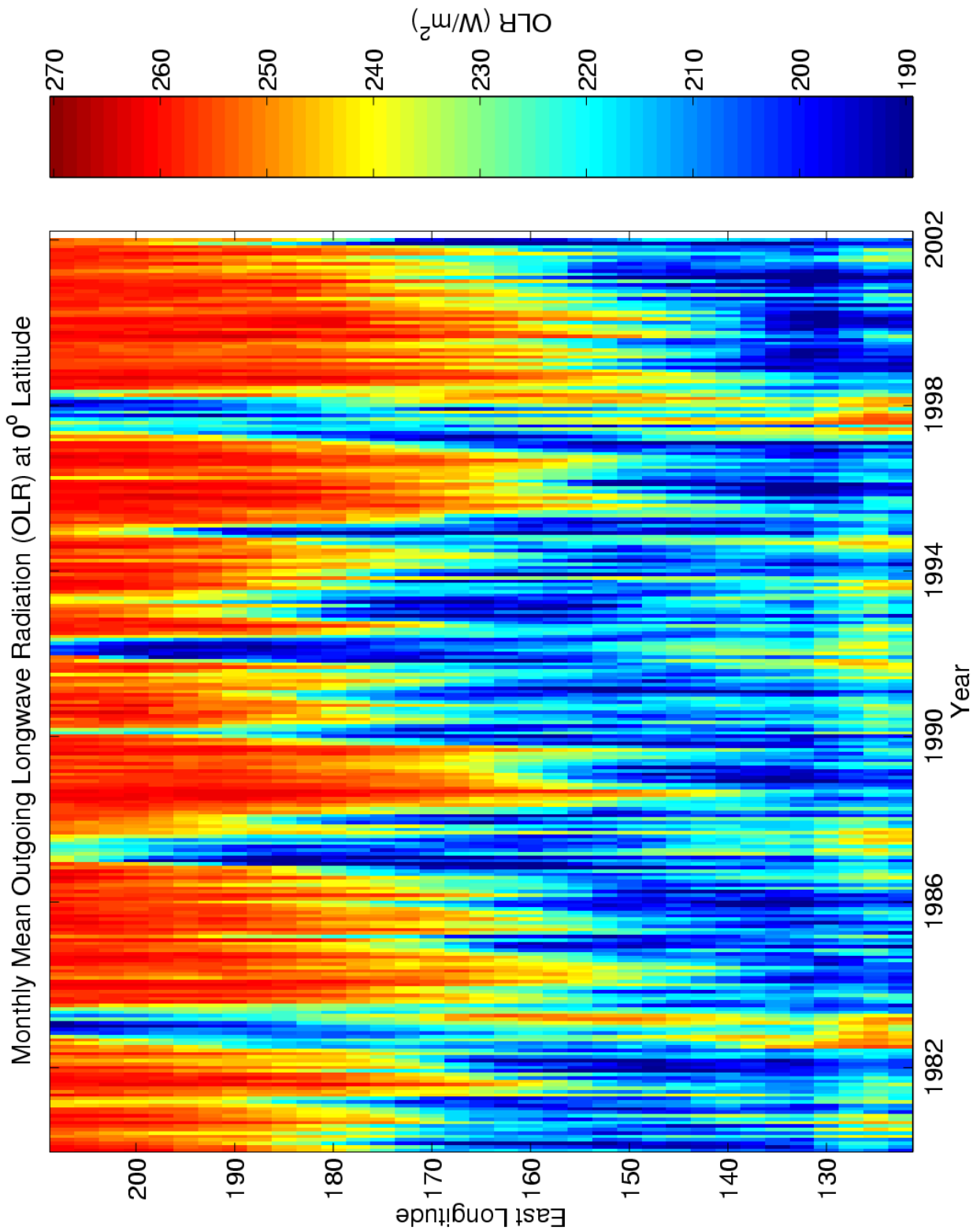


**Figure 1.** Time versus longitude diagram of monthly mean OLR at 0° latitude covering the TWP region. OLR is measured by the geostationary meteorological satellite (GMS).

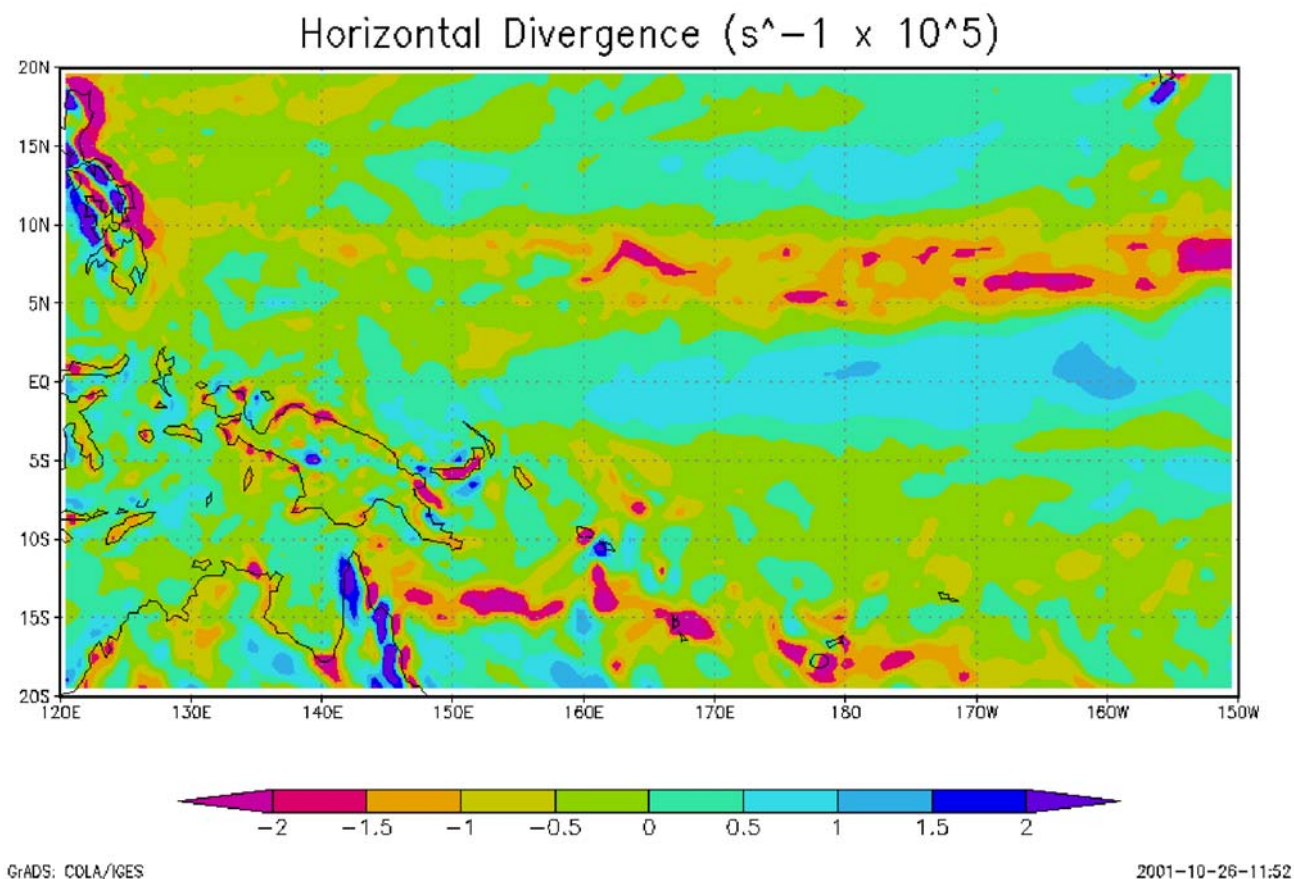


**Figure 2.** Spatial distribution of horizontal divergence in the TWP region. Results are from ECMWF analysis in November 1999 at the 1000-mbar level.

following the South Pacific islands in that region. Manus lies at the intersection of these two convective bands, while Nauru lies in the gap between them. While Nauru is often in a region of suppressed convective activity, horizontal divergence near the tropopause associated with the ITCZ and the SPCZ can provide sources of upper-level moisture to the equatorial convective gap increasing the potential for in situ cirrus formation.

## Radiation Budget

Differences in convective activity at Manus and Nauru can also be illustrated by examining the TOA and surface fluxes. A time series of monthly mean OLR from NCEP analysis data (Figure 3) compares values over Manus and Nauru. During La Nina periods (i.e., 1995-96; 1999-2001), OLR is significantly higher at Nauru than at Manus. During El Nino periods, OLR decreases at Nauru, with lower values than observed at Manus during convective periods.

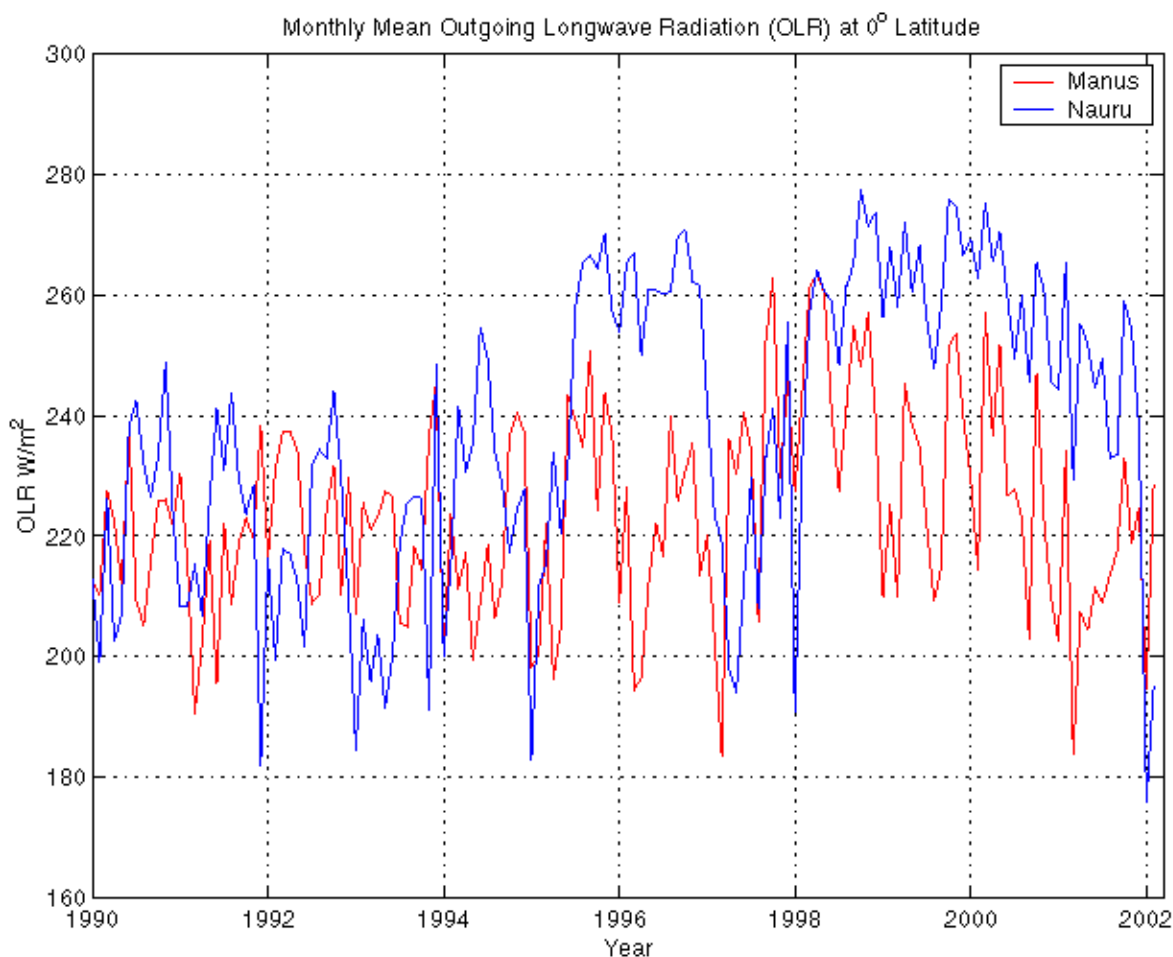


**Figure 3.** Monthly mean OLR derived from NCEP analysis data over Nauru and Manus from 1990-2001.

The El Niño-Southern Oscillation (ENSO) cycle is also observed at the surface. Shortwave cloud forcing (SCF) at Nauru (Figure 4a) exhibits relatively constant behavior until approximately 2001, when SCF increases steadily up to 2002. This may indicate the onset of El Niño as Nauru shifts from a region of suppressed to a region of active convection. Precipitation also increases during 2001 (not shown). At Manus (Figure 4b), the trend in SCF is less distinct because this region is less affected by the ENSO cycle.

## Tropical Cirrus Formation Mechanisms

Two mechanisms are important in the formation of cirrus clouds in the tropics. The first mechanism forms cirrus as a result of outflow from cumulonimbus clouds near the top of convective cells (anvil cirrus). Cloud microphysical properties may vary depending on strength of the convection, temperature, and distance of cirrus from the convective core. Aircraft in situ measurements indicate anvil cirrus can

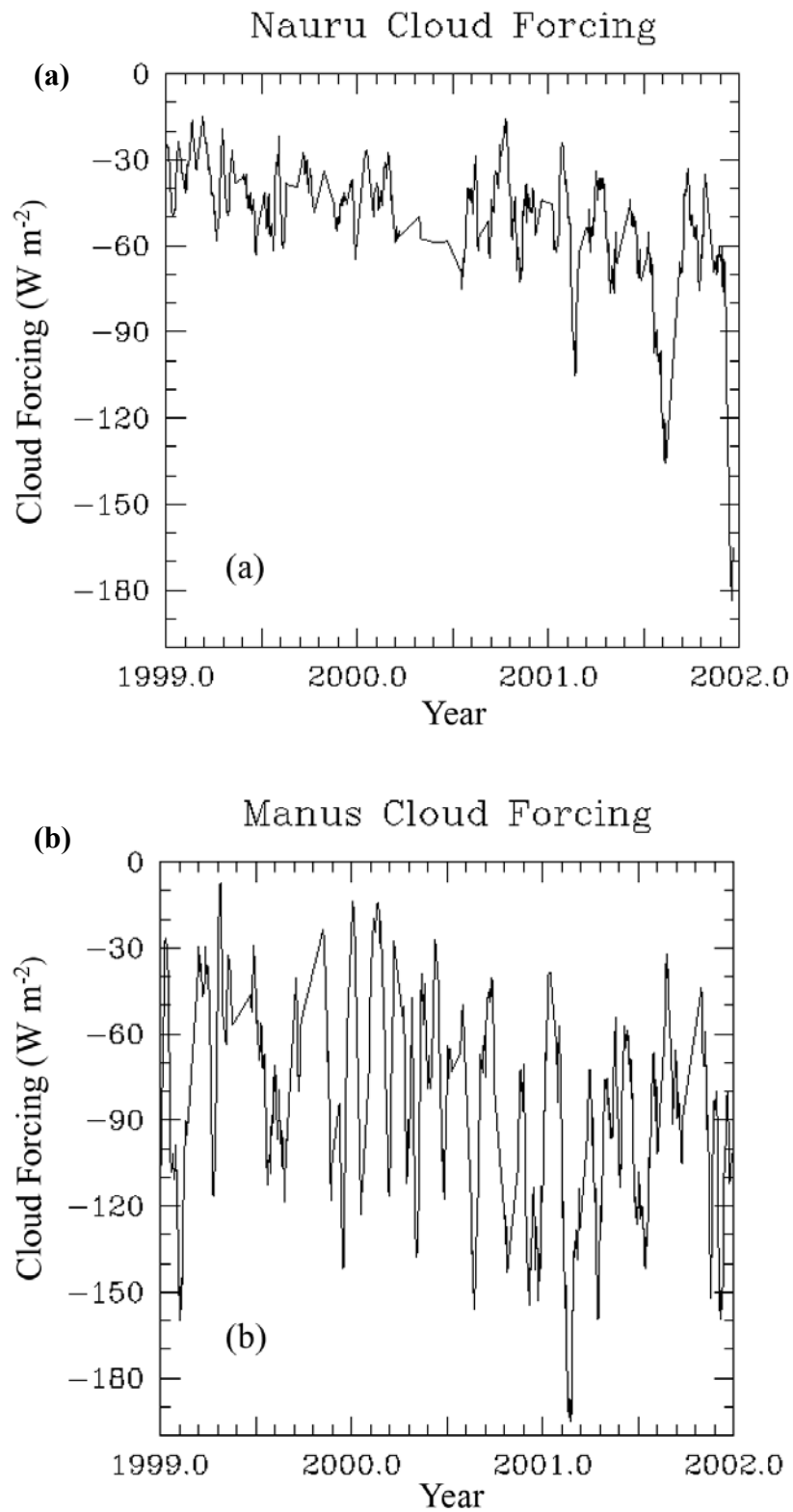


**Figure 4.** Daily averages of SCF measured at the surface in  $\text{W m}^{-2}$  for (a) Nauru and (b) Manus. The data are smoothed using a 10-day running average.

have irregular-shaped ice crystals, particularly at warmer temperatures, higher ice water content, and when sampled near the convective center (Heymsfield and McFarquhar 1996; McFarquhar and Heymsfield 1996).

The second mechanism is cirrus formed by large-scale processes producing thin, laminar clouds located near the tropical tropopause (tropopause cirrus). Observations suggest that tropopause cirrus is not directly associated with local convection but is a separate class from anvil cirrus (Comstock et al. 2002). The exact mechanism that forms tropopause cirrus is uncertain, but cirrus occurrence has been associated with cold temperature perturbations in the upper troposphere that occur as downward propagating Kelvin waves extend from the stratosphere (Boehm and Verlinde 2000). Large-scale uplift has also been suggested as a possible mechanism (Jensen et al. 1996). Little is known about the microphysical properties of tropopause cirrus because it exists above 15 km and is difficult to sample with aircraft probes. In the following section, we examine cirrus cloud properties to help determine the important mechanisms at each site.

## Cloud Properties Statistics

Cloud height, thickness, and visible optical depth,  $\tau$ , are derived from micropulse lidar (MPL) backscatter profiles using the method of Comstock and Sassen (2001). This method uses the above-cloud molecular signal to normalize the backscatter profile, and therefore, is subject to errors as the lidar signal becomes fully attenuated. Due to the low output energy of the MPL, the daytime signal-to-noise ratio is low, increasing uncertainty in daytime retrievals and cloud boundary detection. Lidar measurements will provide optical depth retrievals for nighttime observations and optically thin cirrus clouds ( $\tau < 2$ ) with an uncertainty of  $\sim 24\%$ .

Due to instrument problems, we do not have a significant time period when data are concurrently available at each site. Therefore, we analyze MPL measurements from Nauru in 1999 and from Manus in 2000. Since this time period (1999-2000) corresponds with La Nina, and the time series of SCF (Figure 4) indicates similar conditions at Nauru during both years, we conclude that comparing Nauru 1999 data with Manus 2000 data should give a reasonable representation of this phase of the ENSO cycle at each site.

Frequency of occurrence of cloud base ( $z_b$ ) and top ( $z_t$ ) height (Figure 5) reveals a higher frequency of clouds with  $z_b > 10$  km at Nauru than observed at Manus. However, Manus has a higher frequency of lower clouds with  $z_b < 7$  km, which corresponds with a higher frequency of local convection during this time period. The lidar is likely attenuated for lower, thicker clouds. Therefore,  $z_t$  is the most reliable for clouds with  $z_t > 10$  km (Figure 5a).

Frequency of occurrence of cloud thickness at different heights (Figure 6) displays a higher frequency of thin clouds at Nauru. This is likely due to the higher frequency of convective activity at Manus during this time period, which can restrict the lidar from detecting thin cirrus aloft. When the lidar is able to penetrate to the upper troposphere, it is clear that cirrus clouds near the tropopause are generally thinner. Similar probability distribution functions for cirrus between 10-14 km show how clouds in this region, which are likely dominated by anvil clouds, are typically thicker.

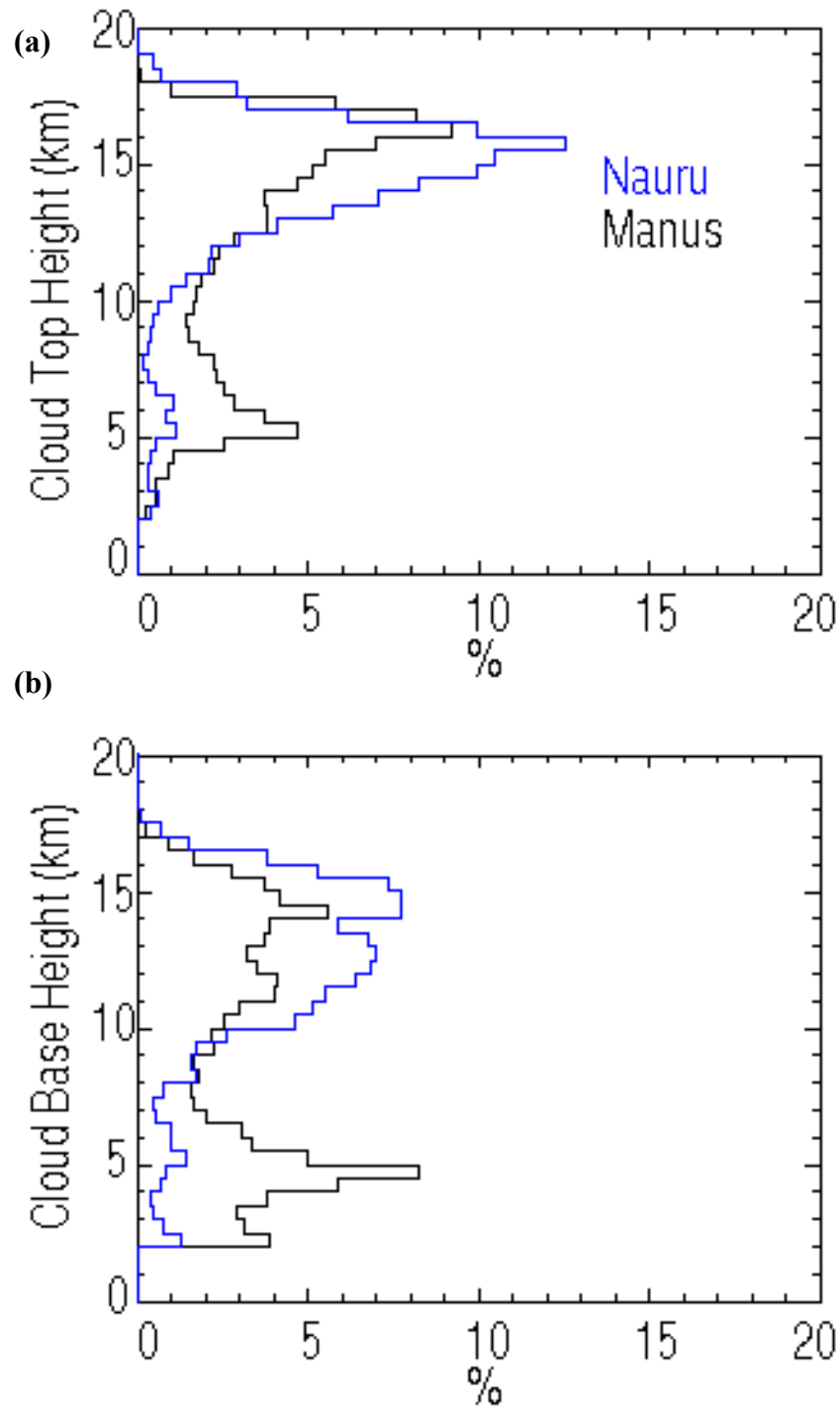


**Figure 5.** Frequency of occurrence of lidar cloud top (a) and base (b) height at Manus and Nauru. Results from Manus are in 2000 and from Nauru in 1999.

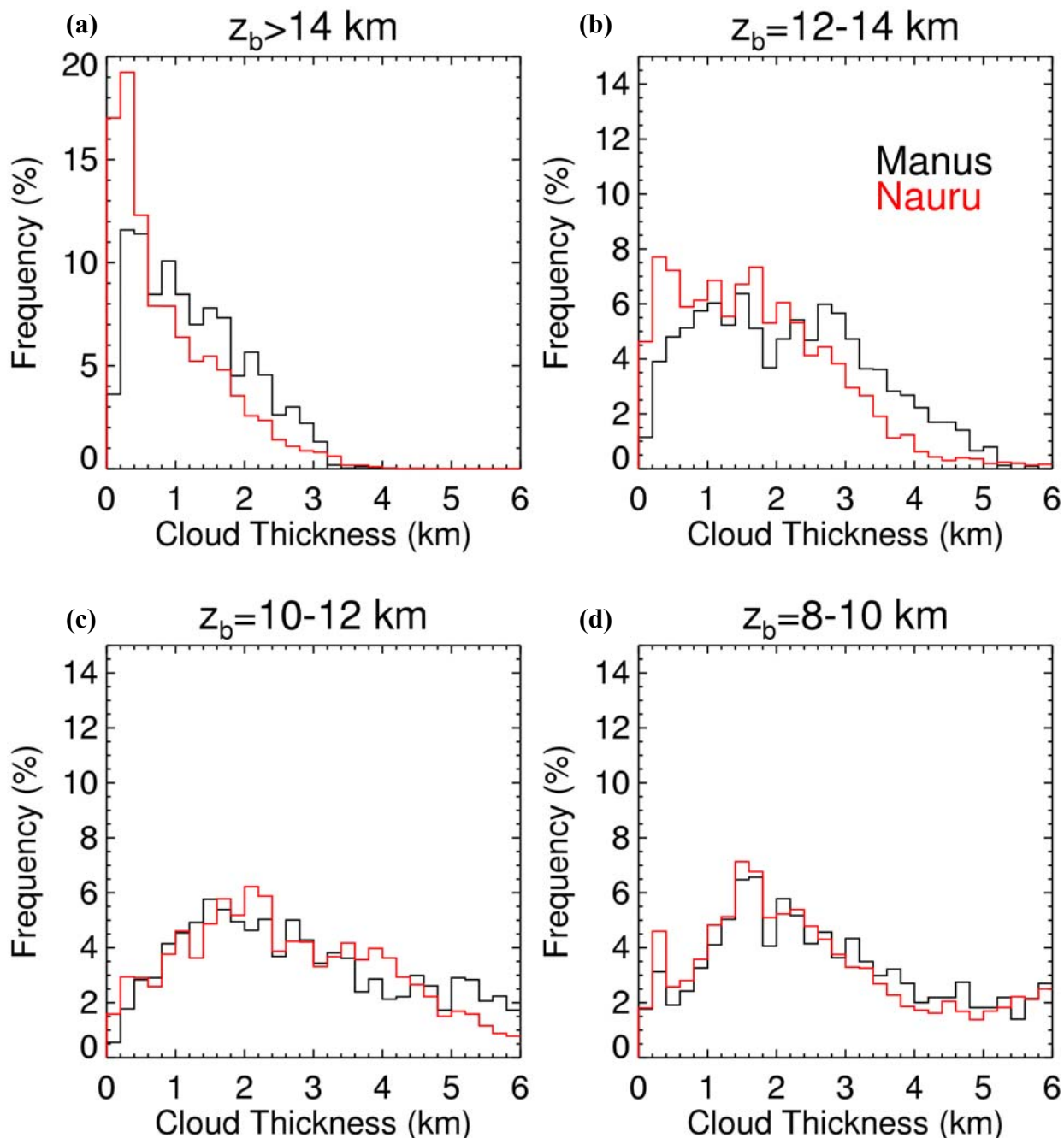


**Figure 6.** Frequency of occurrence of lidar cloud thickness comparing measurements at Manus and Nauru. Cloud thickness is divided into four regions based on cloud base height with (a)  $z_b > 14$  km, (b)  $12 < z_b < 14$  km, (c)  $10 < z_b < 12$  km, and (d)  $8 < z_b < 10$  km. As in Figure 5, results for Manus are from 2000 and Nauru for 1999.

Due to the higher frequency of lower, thicker clouds, it is not surprising that lidar-derived visible optical depth ( $\tau$ , Figure 7) is also larger at Manus. There is a higher frequency of  $\tau > 0.5$  at lower altitudes (8-12 km) observed at Manus, which correlates with a higher frequency of local convection, as seen in the Figure 4. Since local convection rarely occurs at Nauru during this time period, anvil cirrus observations ( $z_b < 15$  km) at Nauru are likely farther away from the convective core and thus have lower optical depths. Cirrus clouds with  $z_b > 14$  km have similar distributions for both sites, illustrating the radiative properties typical of high, tropopause cirrus.

## Thermodynamics

To further characterize the formation mechanisms, we also examine thermodynamic properties at Manus and Nauru. Relative humidity (RH) and RH with respect to ice ( $RH_{ice}$ ) derived from radiosonde data in 2000 is divided into four vertical regions (Figure 8) reveals the distribution of moisture in the tropical atmosphere.  $RH_{ice}$  is calculated when the temperature is less than 233 K. Frequency distributions of  $RH_{ice}$  (Figure 8) between 15-18 km are comparable at each site. This corresponds to similarities in  $\tau$  distributions at this height (Figure 7). Differences in distributions of RH at lower altitudes (0-5 and 5-10 km) demonstrate the contrast in moisture budgets at each location during 2000. Higher RH at Manus is characteristic of local deep convection in that region.

Figure 9 displays temperature anomalies calculated using a 30-day running average at each height level (200-m resolution) between 10-20 km. Each profile represents a 12-hour time period during 2000. Negative temperature anomalies are associated with Kelvin waves propagating downward from the stratosphere (Holton et al. 2001). Boehm and Verlinde (2000) have linked high, laminar cirrus ( $z_b > 15$  km) occurrence with tropical Kelvin waves during the Nauru99 intensive observation period. Although similar patterns in temperature exist at Manus and Nauru (Figure 9), the presence of local convection, as well as seasonal and interseasonal oscillations, will also influence cirrus formation.

## Cirrus Examples

In this section, we present two examples of cirrus that are typically observed in the tropics. The first example is a high cirrus layer lying near the tropical tropopause. The height versus time display of lidar backscattered energy (Figure 10b) observed on May 28, 1999, at Nauru reveals the structure of this cirrus cloud is generally laminar in appearance (0000-0900 Universal Time Coordinates [UTC]), but also exhibits periods of enhanced structure and increased backscattered intensity (0900-1400 UTC). This is also seen in the optical depths (Figure 10c), which range from  $\tau < 0.03$  before 0900 UTC and increase to  $\sim 0.15$  at  $\sim 1200$  UTC. Figure 10b also depicts the high signal-to-noise ratio in the daytime, which decreases the sensitivity of the lidar to the presence of thin cirrus clouds. Radar reflectivity from the millimeter wave cloud radar (MMCR; Figure 10a) does not detect the cirrus layer detected by the lidar but only detects some scattered cumulus in the boundary layer at  $\sim 2100$  UTC. The MMCR has difficulty detecting high, thin cirrus because the ice crystal size is likely very small, combined with a decrease in sensitivity as range increases. In this particular case, cirrus persists over Nauru for nearly 5 days. Imagery from the Japanese GMS indicates that the moisture needed to form this cirrus was

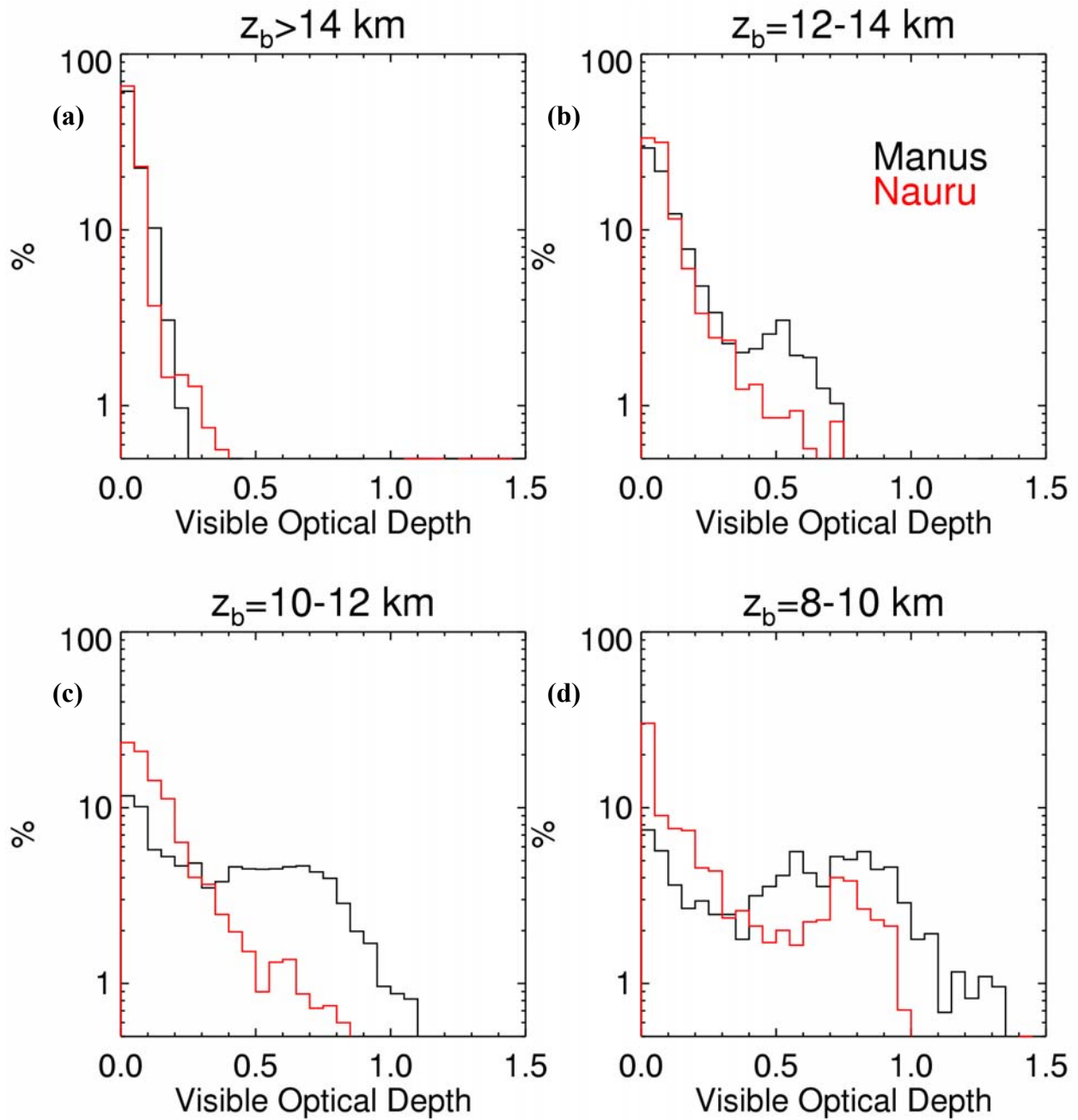


**Figure 7.** Frequency of occurrence of lidar visible optical depth for divided into regions based on cloud base height with (a)  $z_b > 14$  km, (b)  $12 < z_b < 14$  km, (c)  $10 < z_b < 12$  km, and (d)  $8 < z_b < 10$  km. Results from Manus are from 2000 and from Nauru for 1999.

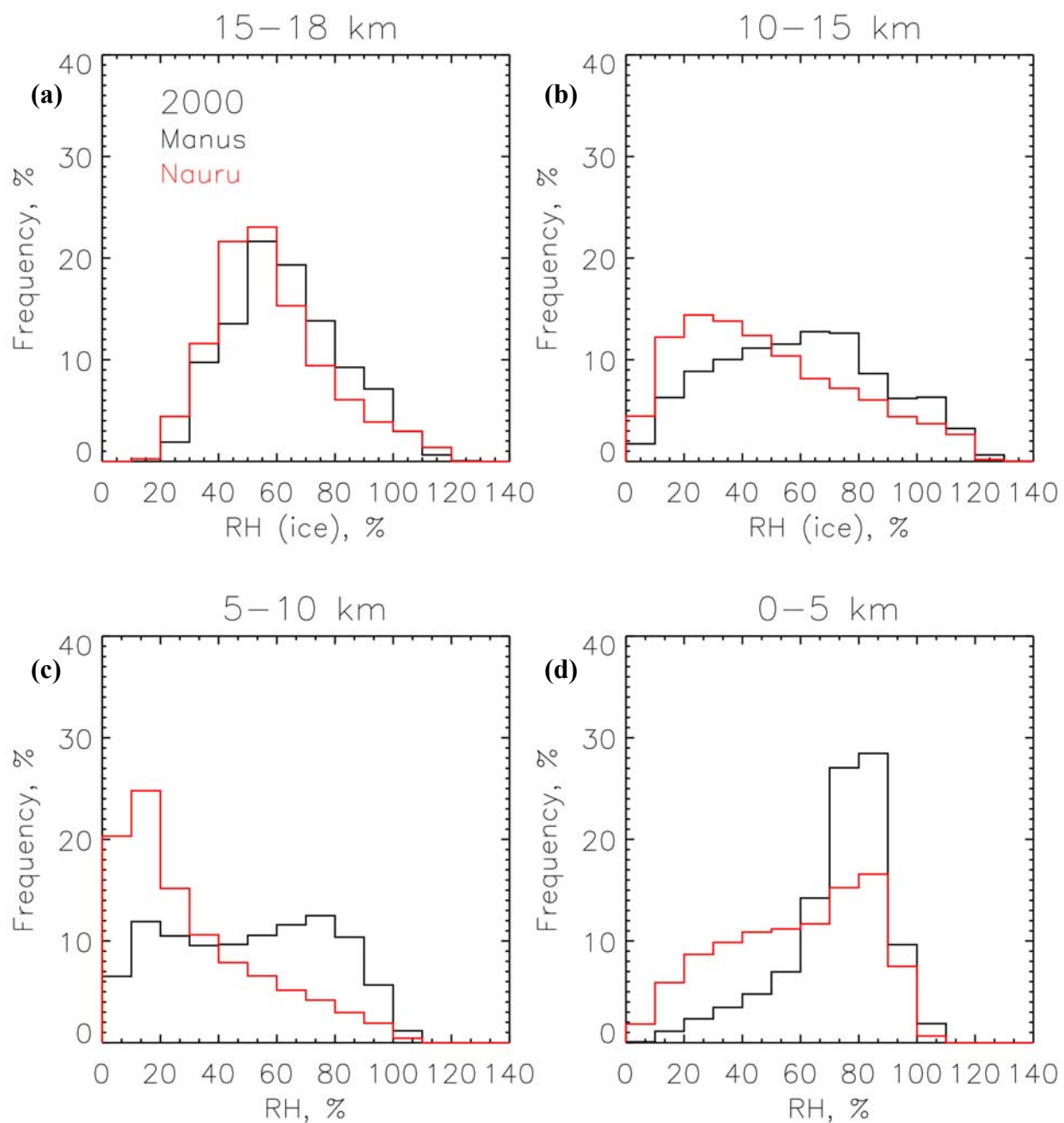


**Figure 8.** Frequency of occurrence of RH and RH<sub>ice</sub> divided into four height regions with (a) 15- 18 km, (b) 10-15 km, (c) 5-10 km, and (d) 0-5 km. This comparison is from radiosonde profiles in 2000.

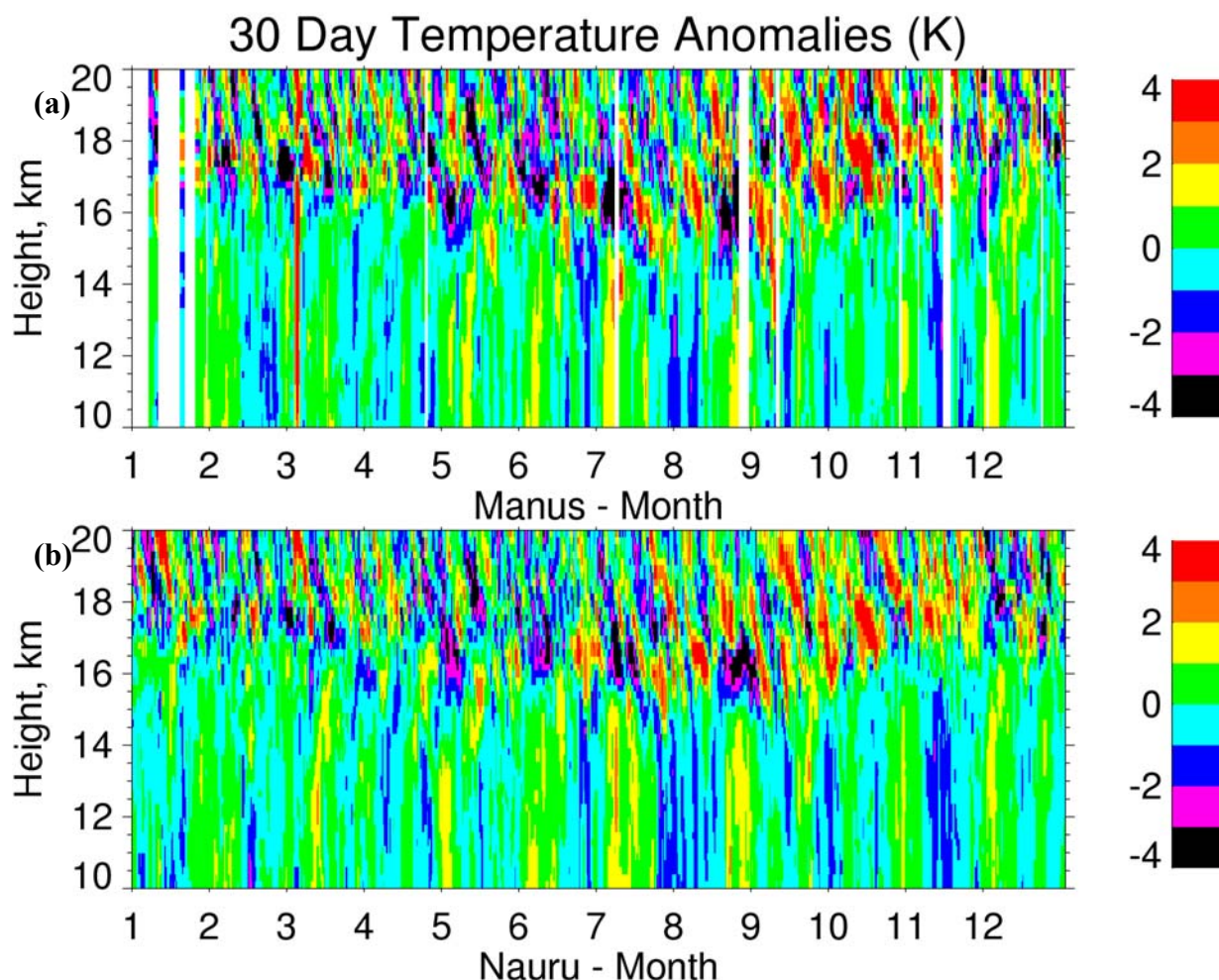


**Figure 9.** Temperature anomalies calculated from radiosonde profiles at Manus (a) and Nauru (b) during 2000. Anomalies are calculated using a 30-day running average at each level.

likely generated by a large convective system located approximately 800 km to the south of Nauru. There is some evidence in the radiosonde data that a cold temperature perturbation exists near the tropopause transition layer on this day, caused by stratospheric waves extending into the upper troposphere. However, the exact mechanism that allows the cirrus to persist for 5 days is still uncertain.

The second example displays a deep convective system observed on March 27, 2000, at Manus. Radar reflectivity (Figure 11a) clearly depicts the passage of the convective cell and the resultant anvil cirrus (0000-1200 UTC). The lidar backscattered intensity (Figure 11b) is attenuation-limited until ~1100 UTC, when a higher cirrus layer becomes visible that is not apparent in radar reflectivities. Due to lidar attenuation,  $\tau$  is underestimated (Figure 11c) and probably greater than 3 in the anvil portion of the cloud. This case exhibits how local convection generates anvil cirrus, as well as the evolution of the cirrus as the convection dissipates. The radiative properties of the anvil also appear to change as the cirrus evolves, with  $\tau$  decreasing as the distance from the convection increases.

### Nauru 28 May 1999

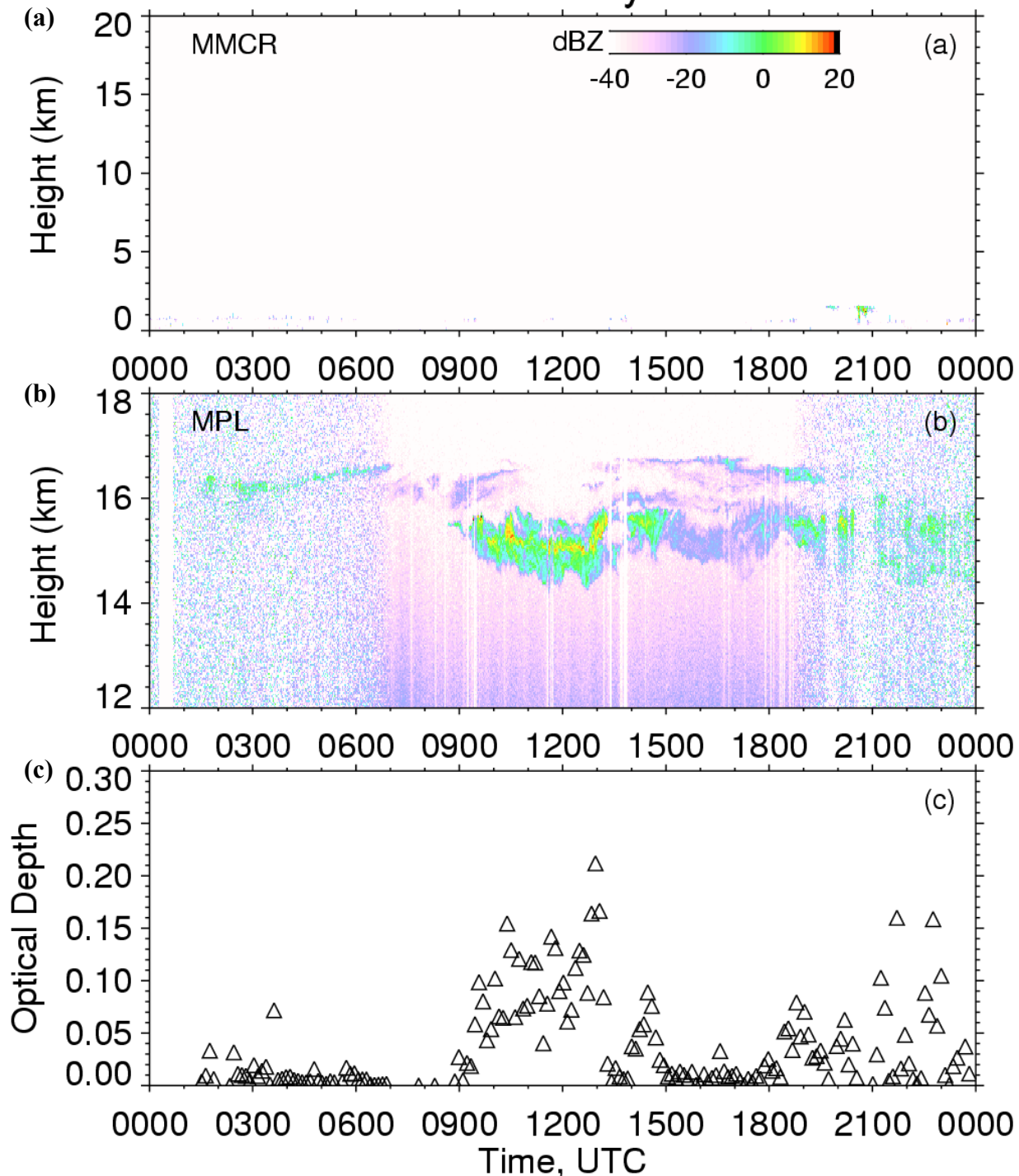


**Figure 10.** Tropopause cirrus observed at Nauru on May 28, 1999. Height versus time display of (a) MMCR radar reflectivity and (b) MPL normalized relative backscatter. Panel (c) displays a time series of lidar visible optical depth.

### Manus 27 Mar 2000

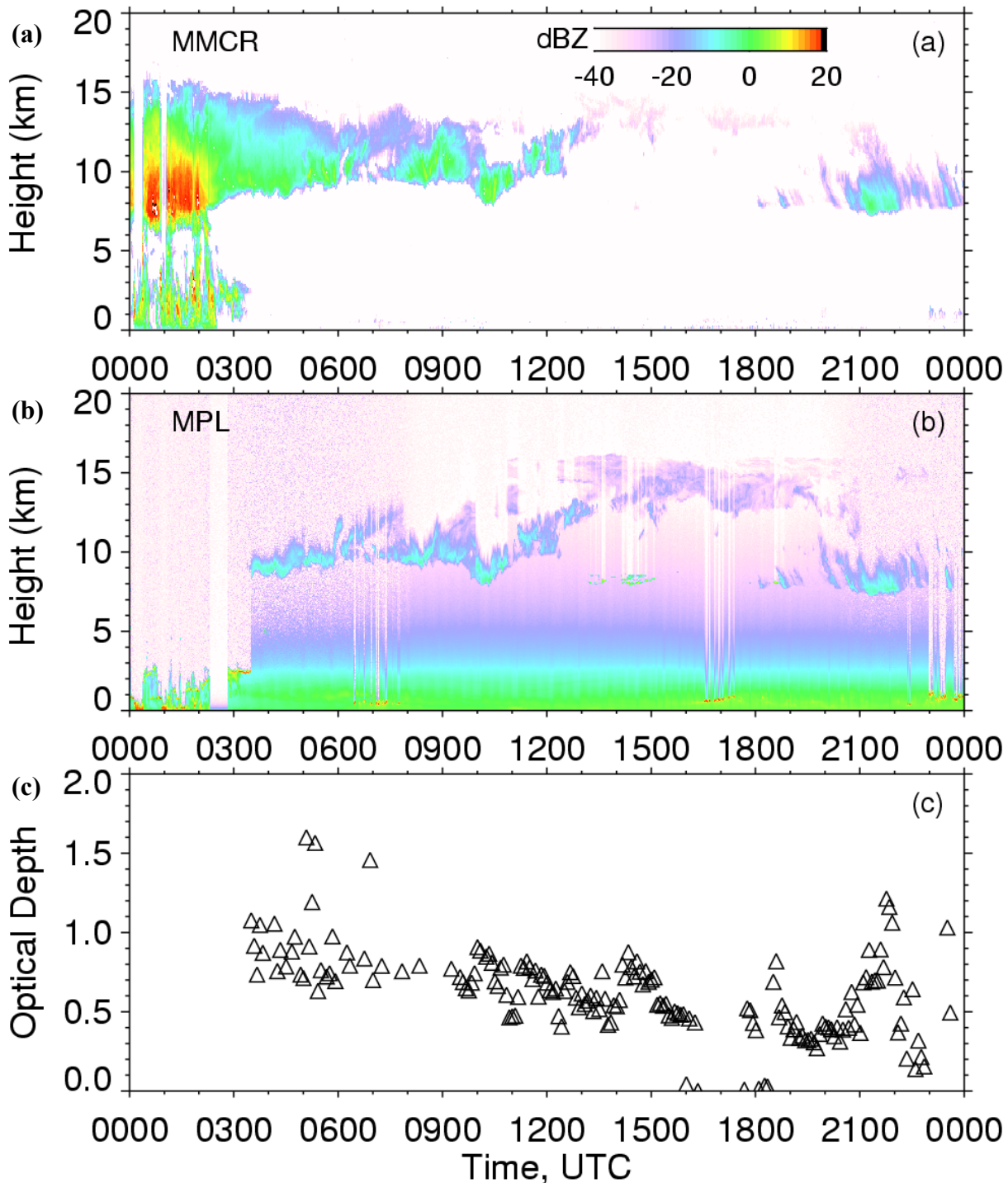


**Figure 11.** Evolution of a convective anvil as it passes over Manus on March 27, 2000. Height versus time display of (a) MMCR radar reflectivity and (b) MPL normalized relative backscatter. Panel (c) displays a time series of lidar visible optical depth.

## Summary

In this study, we compared cloud properties observed at two different locations in the TWP. During this time period, Manus was influenced by local convection, which results in increased frequency of lower, thicker clouds that greatly influence the radiation budget. On the other hand, in 1999 the region around Nauru was convectively suppressed. High cirrus clouds dominate observations, which have a much smaller effect on SCF. These optically thin clouds will influence radiative heating in the upper troposphere (McFarquhar et al. 2000; Comstock et al. 2002) and may play a role in the exchange of water vapor between the stratosphere and troposphere.

We also presented examples of different cirrus formation mechanisms that help illustrate the influence of different cirrus types on the energy budget. Anvil cirrus generated by local convection is often physically and optically thick when observed near the convective center. An extensive cirrus layer that lasted several days appeared to be influenced by stratospheric waves. As illustrated in these examples, various dynamic mechanisms influence cirrus cloud formation in the tropics on various spatial and time scales. These dynamic processes also include the effect of the ITCZ and SPCZ, the Madden-Julian Oscillation, and the quasi-biennial oscillation. Continued research in this area will help us understand the specific mechanisms that allow cirrus to form and persist, and also control stratospheric water vapor in the tropics.

## References

- Boehm, M. T., and J. Verlinde, 2000: Stratospheric influence on upper tropospheric tropical cirrus. *Geophys. Res. Lett.*, **27**, 3209-3212.
- Comstock, J. M., T. P. Ackerman, and G. G. Mace, 2002: Ground-based remote sensing of tropical cirrus clouds at Nauru Island: cloud statistics and radiative impacts. *J. Geophys. Res.*, submitted.
- Comstock, J. M. and K. Sassen, 2001: Retrieval of cirrus cloud radiative and backscattering properties using combined lidar and infrared radiometer (LIRAD) measurements. *J. Atmos. Oceanic Technol.*, **18**, 1658-1673.
- Heymsfield, A. J., and G. M. McFarquhar, 1996: High albedos of cirrus in the tropical Pacific warm pool: microphysical interpretations from CEPEX and from Kwajalein, Marshall Islands. *J. Atmos. Sci.*, **53**, 2424-2451.
- Holton, J. R., M. J. Alexander, and M. T. Boehm, 2001: Evidence for short vertical wavelength Kelvin waves in the Department of Energy-Atmospheric Radiation Measurement Nauru99 radiosonde observations. *J. Geophys. Res.*, **106**, 125-20,129.
- Jensen, E. J., O. B. Toon, H. B. Selkirk, J. D. Spinhirne, and M. R. Schoeberl, 1996: On the formation and persistence of subvisible cirrus clouds near the tropical tropopause. *J. Geophys. Res.*, **101**, 21,361-21,375.

McFarquhar, G. M., and A. J. Heymsfield, 1996: Microphysical characteristics of three anvils sampled during the central equatorial pacific experiment. *J. Atmos. Sci.*, **53**, 2401-2423.